# Active Touch Perception
# Produced by Airborne Ultrasonic Haptic Hologram

Seki Inoue[1], Yasutoshi Makino[2] and Hiroyuki Shinoda[2]

*Abstract*— **A method to present volumetric haptic objects in the air using spatial modulation of ultrasound is proposed. Previous methods of airborne ultrasonic tactile display were based on vibrotactile radiation pressure and sensor feedback systems, which result in low spatial receptive resolution. The proposed approach produces a spatially standing haptic image using stationary ultrasonic waves that enable users to touch 3D images without depending on vibrotactile stimulation and sensor feedback. The omnidirectional spatial modulated haptic images are generated by a phased array surrounding a workspace, which enables enough power to feel shapes without vibrotactile technique. Compared with previous methods, the proposed method can create a completely silent image without temporal ultrasonic modulation noise that is free of the problems caused by feedback delay and errors. To investigate the active touch profiles of an ultrasonic image, this paper discusses a method to synthesize a haptic holographic image, the evaluation of our algorithm, and the results of pressure measurement and subjective experiments.**

## I. INTRODUCTION

Active touch is indispensable in recognition systems to obtain spatial and environmental information, such as shapes, locations, textures, or deformations, from haptic sensations. In contrast to passive touch, which is a pure cutaneous sense, active touch is a combination of cutaneous sensation and proprioception resulting from voluntary motor activity [1]. Recent functional magnetic resonance imaging studies have demonstrated that each type of touch invokes a completely different brain activity and have also considered a temporal processing hierarchy with active touch [2].

Achieving programmable 3D space for active touch has attracted considerable attention. Proxy type devices with robot arms, such as Phantom by Geomagic/SensAble [3] and Falcon by Novint [4] are effective approaches to display forces and kinesthesis. However, the finger form is fixed, which makes tactile expressiveness less flexible. SPIDAR-MF [5] allows free finger motion by assigning a three degree-of-freedom force to each finger individually. Data gloves with force feedback, such as the Ghost Glove [6], can also be used to realize a finger-unconstrained haptic display. However, such approaches require that devices are worn, and finger motion does not provide sufficient preciseness or temporal response for successful haptic feedback.

An emerging possibility is mid-air haptic technology, which requires no direct contact with physical devices. Air jet driven tactile displays [7][8] and ultrasound-based tactile displays have been proposed [9][10][11]. Air jet or vortex based displays have simple structures; however, the spatial and temporal profiles remain rough, at least at this stage. Conversely, focused ultrasonic displays provide small latency and sufficient spatiotemporal resolution [8][10].

Attempts to achieve active touch with airborne ultrasound tactile displays have also been reported. Yoshino et al. [12] and Monnai et al. [13] proposed systems that provided tactile feedback to floating visual touch screens. A single ultrasonic focus was invoked when the sensor recognized a finger touch on a virtual screen. Long et al. [14] proposed a volumetric haptic shape display using ultrasound that created vibrotactile stimulation at the intersection of a palm and a virtual object using optical finger detectors. Here, we discuss some of the limitations of these studies. First, although vibrotactile sensation enhances the intensity of perception, it has quite low spatial properties and is not truly a natural sensation for actual contact. Anatomical and microneurographic studies have shown that, in humans, a single vibrotactile mechanoreceptive unit has a wide receptive field range and low spatial resolution [15]. From an engineering perspective, due to the lack of accurate temporal and spatial resolution in vision based finger motion sensing, current systems choose and reproduce stored vibration data based on relatively rough and slow estimation of the finger position. To produce a vibration faithful to real contact with textures for a quick sliding hand motion, the feedback should have quite high spatial and temporal resolution, which is currently unavailable. Second, sound from the temporal amplitude modulation of the vibrotactile sensation spoils the audio experience when combined with virtual reality systems.

Our previous work has shown that a single focus created by surrounding phased arrays can be perceived as an omnidirectionally pinchable sphere [16]. The perceived sphere has a radius comparable to the focal point.

In this paper, we extend our previous approach to present volumetric haptic objects that utilize ultrasound spatial modulation rather than temporal modulation. A surrounding ultrasonic phased array generates omnidirectionally touchable surfaces, lines, points, and volumetric objects that can be freely touched by a user without sensor feedback. It is also possible for multiple users to share an object on any part of the body. Since skin vibration is produced by the user's motion relative to the spatially modulated stationary waves, no audible noise from temporal modulation occurs.

[1]Seki Inoue is with Graduate School of Information Science and Technology, The University of Tokyo, Tokyo, Japan `seki_inoue@ipc.i.u-tokyo.ac.jp`
[2]Yosutoshi Makino and Hiroyuki Shinoda are with Graduate School of Frontier Sciences, The University of Tokyo, Tokyo, Japan `yasutoshi_makino@k.u-tokyo.ac.jp`, `hiroyuki_shinoda@k.u-tokyo.ac.jp`

This research was partly demonstrated at ACM SIG-GRAPH'14 Emerging Technologies [17] and Asia Haptics 2014 [18], and a preliminary hardware setup was revealed at SICE SII'14 [19]. However, only a demonstration was performed; the technical details have not yet been reported. Furthermore, we improved the algorithm to synthesize a phased array. This paper describes the following: (1) how to synthesize the arbitrary patterns by a surrounding phased array, (2) numerical and measurement experiments for spatially modulated acoustic fields, and (3) subjective experiments of active touch recognition for ultrasonic objects.

## II. PRODUCING 3D RADIATION PRESSURE PATTERN

Phased array technologies and the technique to create an arbitrary wave field have been widely researched, including researches in antenna engineering [20], 3D audio [21], and, even neuroscience [22] fields. The unique key point of our problem is that the magnitude of acoustic radiation pressure is in proportional to the squared sound pressure, which makes the problem nonlinear.

### A. Acoustic Radiation Pressure

Acoustic radiation pressure is a nonlinear phenomenon of intense acoustic wave propagation that generates DC pressure on obstacles in the medium. The radiation force $F$ induced by sound pressure $p$ on boundary $S_0$ approximated as follows:

$$\boldsymbol{F} = \int_{S_0} \alpha \frac{\overline{p^2}}{\rho c^2} d\boldsymbol{S} \tag{1}$$

where $1 \leq \alpha \leq 2$ is a constant that is dependent on the reflection coefficient, $\rho$ is the density of the air and $c$ is the speed of sound in air.

### B. Problem to be Solved

Single frequency acoustic pressure at $\boldsymbol{r}$ generated by a single transducer at $\boldsymbol{r_i}$ with complex gain $q_i$ is expressed as follows:

$$p_i(\boldsymbol{r}) = q_i \frac{D(\theta_i(\boldsymbol{r}))}{|\boldsymbol{r} - \boldsymbol{r_i}|} e^{-(\beta + jk)|\boldsymbol{r} - \boldsymbol{r_i}|} \tag{2}$$

where $D(\theta)$ is the directivity function of a transducer, $\theta_i(r)$ is the angle between the transducer normal and $\boldsymbol{r} - \boldsymbol{r_i}$, $\beta$ is the attenuation coefficient, and $k$ is the wave number. Thus, the wave field generated by a phased array is expressed as follows:

$$p(\boldsymbol{r}) = \sum_i \frac{D(\theta_i(\boldsymbol{r}))}{|\boldsymbol{r} - \boldsymbol{r_i}|} e^{-(\beta + jk)|\boldsymbol{r} - \boldsymbol{r_i}|} q_i \tag{3}$$

$$= \sum_i G_i(\boldsymbol{r}) q_i. \tag{4}$$

Note that we amalgamate the transfer coefficient to $G_i(\boldsymbol{r})$.

By spatially discretizing wave field $p(\boldsymbol{r})$, we obtain the following simple linear equation:

$$\boldsymbol{p} = G\boldsymbol{q} \tag{5}$$

where $p_l = p(\boldsymbol{r}_l)$ and $G_{i,l} = G_i(\boldsymbol{r}_l)$. The discretized points $\boldsymbol{r}_l$ are referred to as control points. This equation describes the generation model of complex pressure at workspace $\boldsymbol{p}$ from phased array complex gain $\boldsymbol{q}$. The linear operator $G$ is fixed by physical arrangement of the transducers. Note that radiation pressure field $a_l^2 = |p_l|^2, a_l \in \mathbb{R}$ is given. Our goal can be summarised as follows:

$$\begin{aligned} \textbf{find} \quad & \boldsymbol{q} \\ \textbf{such that} \quad & a_l = |(G\boldsymbol{q})_l|. \end{aligned} \tag{6}$$

### C. Algorithms to Determine the Driving Signals

Problem (6) is known as phase retrieval, which has been researched in the field of scattering diffraction imaging [23]. A well-known, classical and practical algorithm is the Gerchberg-Saxton (GS) method [24]. Algorithm 1 shows the pseudocode of the GS method, where $G^-$ is the inverse operator of $G$. Here, we chose Tikhonov regularized inverse operator to reduce energy consumption and suppress side-lobes.

---

**Algorithm 1** Gerchberg-Saxton

**Require:** Initial random value : $p^0$ such that $|p_i^0| = a_i$
**Ensure:** $|p_i^N| = a_i = |(G\boldsymbol{q^N})_i|$
    **for** $k = 0$ to $K - 1$ **do**
        $p_i^{k+1} \leftarrow a_i \frac{(GG^-\boldsymbol{p^k})_i}{|(GG^-\boldsymbol{p^k})_i|}$
    **end for**

---

The GS method is quite simple; however, it is known that this greedy algorithm does not to converge well. Recently, Waldspurger et al. proposed a relaxation formulation of a semi-definite programming for the phase retrieval problem [25]. Without going into detail, the relaxed semi-definite programming (SDP) is summarised as follows:

$$\begin{aligned} \textbf{minimize} \quad & \text{Tr}(UM) \\ \textbf{subject to} \quad & \text{diag}(U) = 1, \ U \succeq 0 \end{aligned} \tag{7}$$

where $M = \text{diag}(\boldsymbol{a})(I - GG^-)\text{diag}(\boldsymbol{a})$. We then obtain $\boldsymbol{q} = G^- \text{diag}(\boldsymbol{a})\boldsymbol{u}$, where $\boldsymbol{u}$ is a leading eigenvector of $U$.

To solve this SDP efficiently, we employ the block coordinate decent method (Algorithm 2), where $i^c$ is the index set $i^c = [1, n] \backslash \{i\}$ and $\mu$ is referred to as the barrier parameter.

We discuss the evaluation of both methods by numerical simulation in section III-B.

## III. DEVICE DESIGN AND EVALUATION

### A. Implementation

The requirements of our system are as follows: (1) an ultrasonic wave should arrive at the workspace omnidirectionally, (2) it should have large aperture for total power and small focal radius, (3) the angles between the workspace and transducers should be minimized, and (4) the user's hand and optional optical images should be reachable. To satisfy these requirements, we employed and implemented an octagonal-prism type phased array. Its appearance from the user's view and its geometry are shown in Fig.1 and Fig.2, respectively.

**Algorithm 2** Block Coordinate Descent Algorithm for Phase Retrival

**Require:** Initial value : $U^0 = I_n$ and $\mu > 0$ (small valued parameter)

**Ensure:** $U \succeq 0 \; with \; \mathrm{diag}(U) = 1$

    **for** $k = 0$ **to** $K - 1$ **do**

        Pick $i \in [1, n]$.

        $x \leftarrow U^k_{i^c, u^c} M_{i^c, i}$.

        $\gamma \leftarrow x^* M_{i^c, i}$.

        **if** $\gamma > 0$ **then**

            $U^{k+1}_{i^c, i} = U^{k+1*}_{i, i^c} = -\sqrt{\frac{1 - \mu}{\gamma}} x$

        **else**

            $U^{k+1}_{i^c, i} = U^{k+1*}_{i, i^c} = 0$

        **end if**

    **end for**

A T4010A1 (developed by Nippon Ceramic Co., Ltd.) was employed as the transducer. The T4010A1 emits 40-kHz ultrasound at 121.5 dB in S.P.L at 30-cm distance. Its angle of directivity is $50°$. It is equipped with 3984 transducers, 80 field-programmable gate array processors, and a USB controller that controls the transducers individually from a PC. Note that each transducer was driven by pulse width modulation (PWM). The relational 40-kHz AC voltage $V$ and PWM duty cycle $D$ is expressed as follows:

$$V = \frac{2}{\pi} V_0 \left| \sin \pi D \right| \tag{8}$$

where $V_0 = 24$V in this setup. The resolutions of the amplitude duty cycle and phase are both 256 levels.

The GS method (Algorithm 1) and SDP+BCD method (Algorithm 2) are implemented with $\mu = 0.1$. Here, the directivity function $D(\theta)$ is approximated by cubic spherical harmonics, and its coefficients from zero-order to third-order are 1.11, 1.06, 0.24, and -0.12.

The control points are sampled from polygon models to satisfy every two points are apart by the wavelength.

*B. Numerical Algorithm Evaluation*

Figures 3 and 4 show the simulated acoustic pressure distributions of a star-bordered surface with the GS method and SDP method, respectively (after 1000 iterations for full convergence). The gray lines indicate the original polygon model, whose vertices were configured as control points with the same amplitude. With the GS method, the shape was not well converged, and a biased distribution was observed. In contrast, the shape was kept symmetrical and clear with the SDP method.

Thus, we concluded that the SDP method is more efficient and robust than the GS method. Therefore,we employed the SDP method.

*C. Acoustic Pressure Measurement*

To measure an actual pressure distribution, we built an auto-measuring instrument that consists of a standard microphone, an amplifier, a 3-axis motorized stage, a digital
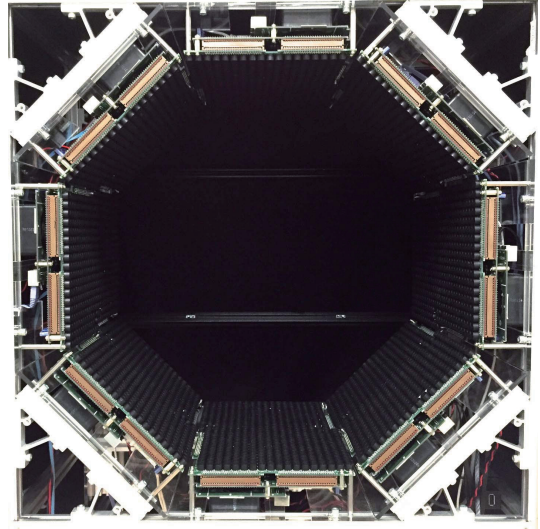


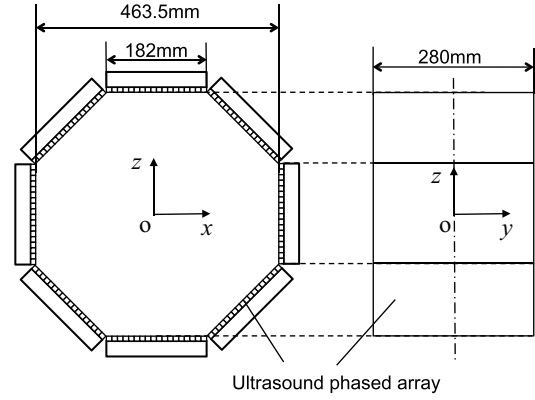Fig. 1. User's view of the octagonal-prism type phased array



Fig. 2. Geometry of the octagonal-prism type phase array (the origin is placed at the center of the cavity)

oscilloscope, and a host PC. Figure 5 shows an overview of the auto-measuring system.

We measured the peak pressure with single focus at the center of the cavity. Note that we could not measure the full power of this device due to the saturation of the microphone. Therefore, all transducers were driven at 20% amplitude, i.e., 32/255 in PWM duty cycle. By 3D measurement with 0.4-mm interval, the peak pressure was revealed as $5.53 \times 10^3$Pa $= 169$ dB SPL.

Without considering the nonlinear acoustic saturation, the rough estimation of the full powered acoustic pressure was $2.77 \times 10^4$Pa $= 182$ dB SPL. According to this estimation, the acoustic radiation force onto a 1-cm$^2$ plane with this acoustic pressure is approximately 100-gw ($\alpha = 2$ in Eq.1). We concluded that this system had sufficient power to present a volumetric feel-able object. Note that this force will not occur for a volumetric surface due to the dispersed pressure distribution.
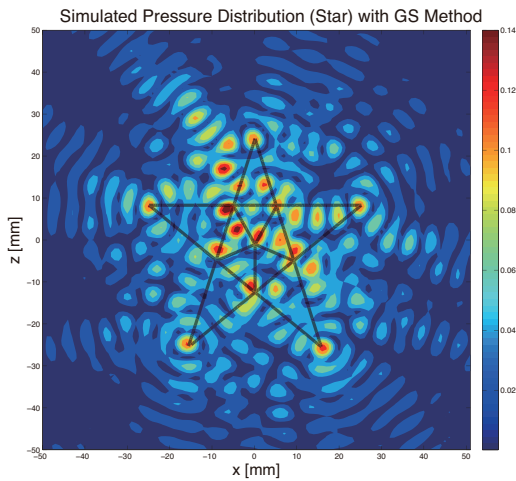
A simple line (34-mm length and 5 control points) was

Fig. 3. Simulated acoustic pressure distribution of a star produced by the GS method with 11 control points (gray lines indicate the original polygon model of the star)
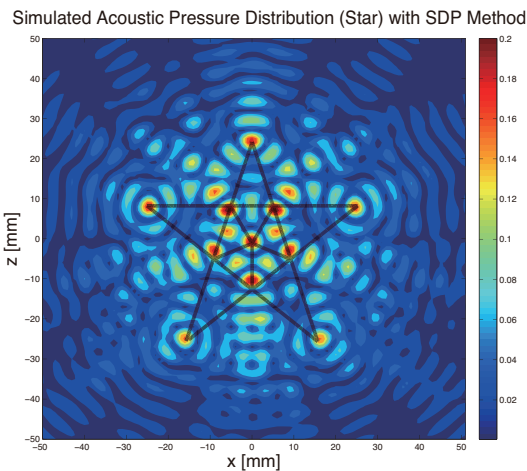


Fig. 4. Simulated acoustic pressure distribution of a star produced by the SDP method with 11 control points (gray lines indicate the original polygon model of the star)

produced, as shown in Figure 6. Note that undesired side-lobes were observed, (approximately 10-mm thicknesses). However, the control points were clearly observable. The side-lobes can be suppressed by tuning the Tikhonov regularization weight parameter. Figure 7 shows a star shaped distribution. The form was somewhat distorted compared with simulated result; however, the correct outline was observable. This is likely due to the following: (1) an error in the physical setup and an individual differences among the transducers, (2) the effect of the microphone (it has an approximately 2-mm diameter) on the ultrasonic field.

## IV. EXPERIMENT

To clarify the active touch sensational profile of ultrasonic primitive objects, we designed two experiments to investi-
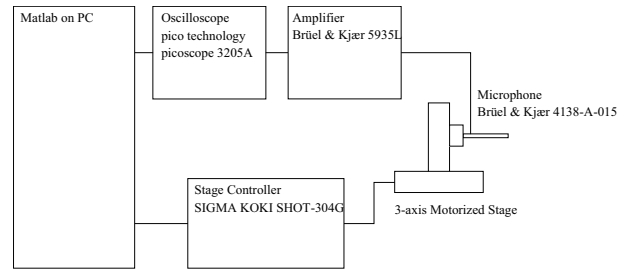


Fig. 5. Overview of the auto measuring system (standard microphone, amplifier, 3-axis motorized stage, digital oscilloscope, and host PC)
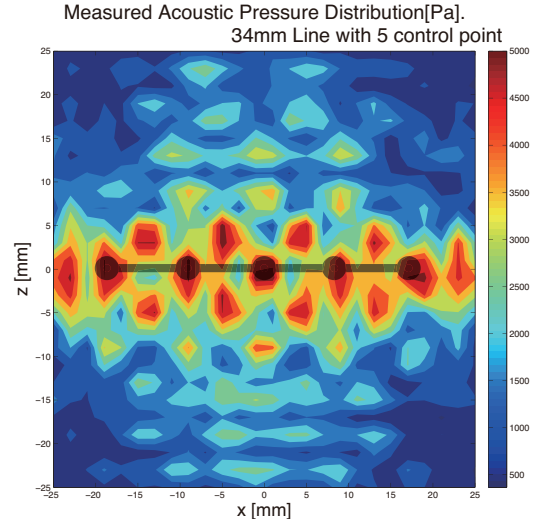


Fig. 6. Measured acoustic pressure distribution displaying a line of 34-mm length with five control points (gray line indicates the desired control points). Note that the color-mapped value is not radiation pressure but the absolute sound pressure at 20% output.

gate the just noticeable differential (JND) of the angle and position of a displayed line. We designed protocols that permitted subjects to act as freely as possible to investigate the realization of intuitive active touch recognition. Thirteen participants (all males, age 22-30) were involved in the both the experiments.

*1) Experiment 1 (Angle JND):* An oblique 100-mm length ultrasonic line $(-50\sin\theta, 0, -50\cos\theta)$ : $(-50\sin\theta, 0, 50\cos\theta)$ is presented. Here, $\theta$ is $0°$ to $45°$ at a $5°$ interval. A height adjustable chair is placed in front of the workspace. Note that subjects are permitted to freely adjust the height of the chair or stand during the experiment. The subjects wear earplugs to avoid receiving hints from the device, such as radiator fan noise. The subject's field of view is not restricted, and the transducer grid is seen as Figure 1. We ask the subjects to move their hand to seek "as they would for a rigid object". Note that the subjects are permitted to use either or both hand. For each trial, the reference angle $\theta = 0$ is presented within 5 seconds and the target angle $0 \leq \theta \leq 45°$ is presented within 15 seconds. Each time the angle/location of the line is changed, the subjects are asked to
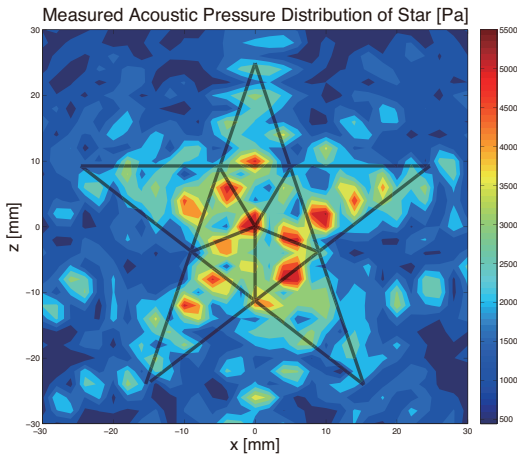
Fig. 7. Measured acoustic pressure distribution of a star produced by 11 control points (gray lines indicate the original polygon model of the star). Note that the color-mapped value is not radiation pressure but sound pressure at 20% output.
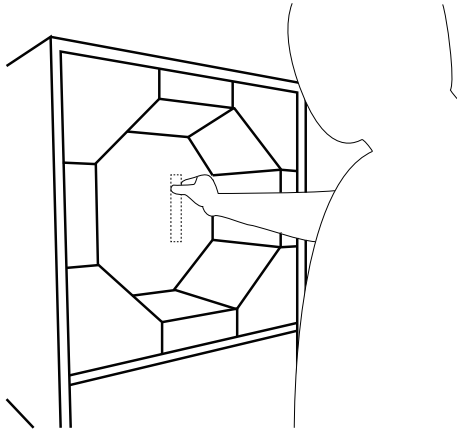


Fig. 8. Illustration of subjective experimental scene. The subject inserts their hand into the cavity and touches or strokes virtual lines.

take their hands out of the device. The subjects are then asked to answer whether the reference and target lines are in the same direction or not. Note that the subjects are permitted to answer at any time before the time is up. In this experiment, a staircase procedure is used. Starting from the maximum angle ($45°$), an alternating descending and ascending series are performed three times. The experiment scene is illustrated in Figure 8.

*2) Experiment 2 (Position JND):* A vertical ultrasonic line (100-mm length) with horizontal translation $(x, 0, -50)$ : $(x, 0, 50)$ is generated. $x$ is shifted from 0 to 27-mm at 3-mm interval. For each trial, the reference location $x = 0$ is presented within 5 seconds and the target location $0 \leq x \leq 27$ is presented within 15 seconds. The other configurations and protocols of this experiments are the same as those in Experiment 1.

*3) Results and Discussion:* Figures 9 and 10 shows the results from the 13 participants. The bold line shows the
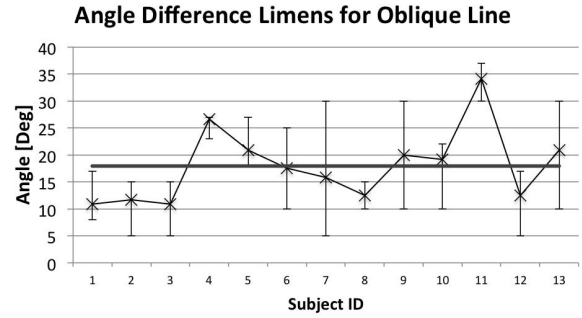


Fig. 9. Angle difference limen for oblique line among all participants. The bold line shows the average angle ($17.9\pm6.6°$).

average angle/distance among all subjects. The upper error bar shows the maximum angle/distance that was reported to be the same, and lower error bar shows the minimum angle/distance that was reported to be different.

Although there are some participants who could identify approximately $10°$, one participant could not identify $30°$. Because we intentionally did not provide specific instructions about how subjects should interact with the system, participant #11 may not have been able to determine an effective way to recognize the shape to the last. For this subject, the method to recognize the angle of an ultrasonic line was not the same as that for a rigid line. In contrast, other participants seemed to comprehend the virtual object quickly and showed good results (participants #1, #2, #3, #8, and #12). The mean JND among all participants was $17.9\pm6.6°$.

Gentaz et al. studied the perception of the orientation of an actual rod [26]. In that study, participants were asked to position a freely rotating rod to a vertical orientation along the frontal plane. The absolute error of the reproduced angle was $3.8° \pm 2.0°$. Note that study attempted to clarify the precision of an angle reproduction task, which is not identical to our task which attempted to clarify a discrimination ability of the presented angles. Thus, these results are not directly comparable; however, the ultrasonic haptic images appear to have somewhat lower property.

Recognizing difference in position appeared to be a much easier task compared to recognizing differences in angle. Both the mean (10.4-mm) and standard deviation (2.5-mm) were close to the line thickness, which was approximately 10-mm (Fig.6).

These results suggest the resolution of psychological haptic imagery created by an acoustic radiation pressure field. We consider that the perceptual spatial resolution of an ultrasonic line is near that of the acoustical resolution of an ultrasonic line. Note that this should be impossible to determine using a vibrotactile approach because the corresponding single receptor (FA II) has a wide ranging receptive field that covers nearly half of the palm [15].

## V. CONCLUSIONS

We have presented a volumetric haptic display that utilizes the spatial modulation of ultrasound to realize an active
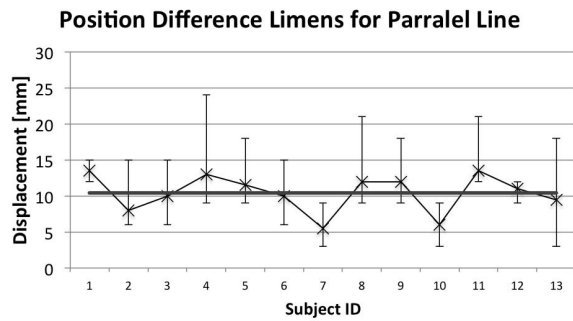
**Position Difference Limens for Parralel Line**

Fig. 10.  Position difference limen for parallel line among all participants. The bold line shows the average displacement across subjects (10.4±2.5mm).

touch environment. In the proposed display system, a surrounding ultrasonic phased array generates omnidirectionally and stationary touchable volumetric objects without sensor feedback. We have also proposed and evaluated a robust and efficient algorithm to determine transducer output. User studies of angle and position JND for a 50-mm virtual line showed a mean angle JND of 17.9±6.6° and a mean of position JND of 10.4±2.5-mm. Note that both results are consistent with the dispersion of the wave distribution.

*Limitations and Further works*

First, the spatial resolution is restricted by the ultrasound wavelength (currently 8.5-mm). Higher frequency ultrasound can improve resolution but the workspace may become smaller due to the attenuation factor.

Second, the presentation of a dynamic object requires remote sensors for feedback. However, to satisfy haptics latency profiles, we would require sensors that function much faster than those designed for graphics applications.

Third, undulated patterns (Fig. 6) of a wave field spoils the tactile experience. While it is possible to change the smoothness of a surface by arranging control point sampling, there is a trade-off between smoothness and intensity. Long's algorithm makes full-undulated patterns in return for the powerful vibrotactile intensity [14].

Finally, additional user studies with more complex objects, as well as comparative evaluation of real objects and ultrasonic objects, are necessary.

## ACKNOWLEDGMENT

## REFERENCES

[1] J. J. Gibson, "Observations on active touch." *Psychological Review*, vol. 69, no. 6, pp. 477–491, 1962.
[2] L. B. Hinkley, L. A. Krubitzer, S. S. Nagarajan, and E. A. Disbrow, "Sensorimotor integration in s2, pv, and parietal rostroventral areas of the human sylvian fissure," *Journal of neurophysiology*, vol. 97, no. 2, pp. 1288–1297, 02 2007.
[3] Geomagic, "Geomagic haptics," http://www.geomagic.com/.
[4] NOVINT, "Falcon," http://www.novint.com/index.php/novintfalcon.
[5] L. Liu, S. Miyake, K. Akahane, and M. Sato, "Development of string-based multi-finger haptic interface spidar-mf," in *Artificial Reality and Telexistence (ICAT), 2013 23rd International Conference on*, Dec 2013, pp. 67–71.
[6] K. Minamizawa, S. Kamuro, N. Kawakami, and S. Tachi, "A palm-worn haptic display for bimanual operations in virtual environments," in *Haptics: Perception, Devices and Scenarios*, ser. Lecture Notes in Computer Science, M. Ferre, Ed.   Springer Berlin Heidelberg, 2008, vol. 5024, pp. 458–463.
[7] Y. Suzuki and M. Kobayashi, "Air jet driven force feedback in virtual reality," *Computer Graphics and Applications, IEEE*, vol. 25, no. 1, pp. 44–47, 2005.
[8] R. Sodhi, I. Poupyrev, M. Glisson, and A. Israr, "Aireal: Interactive tactile experiences in free air," *ACM Trans. Graph.*, vol. 32, no. 4, pp. 134:1–134:10, July 2013.
[9] T. Iwamoto, M. Tatezono, and H. Shinoda, "Non-contact method for producing tactile sensation using airborne ultrasound," in *Haptics: Perception, Devices and Scenarios*.   Springer, 2008, pp. 504–513.
[10] T. Hoshi, M. Takahashi, T. Iwamoto, and H. Shinoda, "Noncontact tactile display based on radiation pressure of airborne ultrasound," *Haptics, IEEE Transactions on*, vol. 3, no. 3, pp. 155–165, 2010.
[11] T. Carter, S. A. Seah, B. Long, B. Drinkwater, and S. Subramanian, "Ultrahaptics: Multi-point mid-air haptic feedback for touch surfaces," in *Proceedings of the 26th Annual ACM Symposium on User Interface Software and Technology*, ser. UIST '13.   New York, NY, USA: ACM, 2013, pp. 505–514.
[12] K. Yoshino and H. Shinoda, "Visio-acoustic screen for contactless touch interface with tactile sensation," in *World Haptics Conference (WHC), 2013*, April 2013, pp. 419–423.
[13] Y. Monnai, K. Hasegawa, M. Fujiwara, K. Yoshino, S. Inoue, and H. Shinoda, "Haptomime: Mid-air haptic interaction with a floating virtual screen," in *Proceedings of the 27th Annual ACM Symposium on User Interface Software and Technology*, ser. UIST '14.   New York, NY, USA: ACM, 2014, pp. 663–667.
[14] B. Long, S. A. Seah, T. Carter, and S. Subramanian, "Rendering volumetric haptic shapes in mid-air using ultrasound," *ACM Trans. Graph.*, vol. 33, no. 6, pp. 181:1–181:10, Nov. 2014.
[15] R. S. Johansson and ke B. Vallbo, "Tactile sensory coding in the glabrous skin of the human hand," *Trends in Neurosciences*, vol. 6, no. 0, pp. 27 – 32, 1983.
[16] S. Inoue and H. Shinoda, "A pinchable aerial virtual sphere by acoustic ultrasound stationary wave," in *Haptics Symposium (HAPTICS), 2014 IEEE*, Feb 2014, pp. 89–92.
[17] S. Inoue, K. J. Kobayashi-Kirschvink, Y. Monnai, K. Hasegawa, Y. Makino, and H. Shinoda, "Horn: The hapt-optic reconstruction," in *ACM SIGGRAPH 2014 Emerging Technologies*, ser. SIGGRAPH '14.   New York, NY, USA: ACM, 2014, pp. 11:1–11:1.
[18] S. Inoue, K. J. Kobayashi-Kirschvink, Y. Furuyama, H. K. Kumagai, Soichiro, and H. Shinoda, "Horn: Stationary airborne ultrasound 3d haptic image," in *Asia Haptics 2014*, 2014.
[19] S. Inoue, Y. Makino, and H. Shinoda, "Designing stationary airborne ultrasonic 3d tactile object," in *System Integration (SII), 2014 IEEE/SICE International Symposium on*, Dec 2014, pp. 159–162.
[20] R. Mailloux, *Phased Array Antenna Handbook*, ser. Antennas and Propagation Library.   Artech House, 2005.
[21] A. J. Berkhout, D. de Vries, and P. Vogel, "Acoustic control by wave field synthesis," *The Journal of the Acoustical Society of America*, vol. 93, no. 5, pp. 2764–2778, 1993.
[22] Y. Hertzberg, O. Naor, A. Volovick, and S. Shoham, "Towards multifocal ultrasonic neural stimulation: pattern generation algorithms," *Journal of Neural Engineering*, vol. 7, no. 5, p. 056002, 2010.
[23] R. W. Harrison, "Phase problem in crystallography," *J. Opt. Soc. Am. A*, vol. 10, no. 5, pp. 1046–1055, May 1993.
[24] R. W. Gerchberg and W. O. Saxton, "A practical algorithm for the determination of the phase from image and diffraction plane pictures," *Optik*, vol. 35, pp. 237–246, 1972.
[25] I. Waldspurger, A. D'Aspremont, and S. Mallat, "Phase Recovery, MaxCut and Complex Semidefinite Programming," June 2012.
[26] E. Gentaz and Y. Hatwell, "Role of gravitational cues in the haptic perception of orientation," *Perception & Psychophysics*, vol. 58, no. 8, pp. 1278–1292, 1996.